Forces in Mechanics 11 (2023) 100186

Contents lists available at ScienceDirect

Forces in Mechanics

journal homepage: www.sciencedirect.com/journal/forces-in-mechanics

Preliminary evaluation of the climate-induced fatigue in wood: A physical and computational approach

A. Califano [a,b], A. Zanola [c], I. Di Terlizzi [d], M. Baiesi [a], C. Bertolin [b,*]

[a] Department of Physics and Astronomy "Galileo Galilei", University of Padua, Padua, Italy
[b] Department of Mechanical and Industrial Engineering, Norwegian University of Science and Technology (NTNU), Trondheim, Norway, Europe
[c] Department of Neurosciences, University of Padua, Padua, Italy
[d] Max Planck Institute, Dresden, Germany

ARTICLE INFO

Keywords:
Wood
Microclimate
Climatic fatigue
Fatigue life
Data-driven

ABSTRACT

Wood is the organic hygroscopic material for excellence. Due to its extremely easy handling, it has always been used in many applications, especially as building material for artefacts and works of art. However, it is highly climate-susceptible as it swells or shrinks by exchanging moisture with the surrounding environment when natural or artificial microclimatic fluctuations occur. The shrinkage/swelling of wood, if repeated over time, may cause the arising of deformations or damage that may lead to catastrophic failures. For this reason, in this work, a preliminary study about the effect that repeated microclimatic loads have on wooden samples is carried out. To do so, well-established fatigue approaches have been implemented, with few simplifying considerations. The case study is a slice of *Scots pine* which is assumed to be stored inside Ringebu stave church (Norway). Ringebu indoor microclimate is reconstructed, through a proper transfer function, starting from outdoor temperature data downloaded from web platforms. The reconstructed indoor temperature timeseries cover three periods: far past (1948–1977), recent past (1981–2010) and far future (2071–2100). The results obtained for the three periods made it possible to gain insights about the climate-induced fatigue of wood and to preliminary assess the impact of climate change. It has been observed that successive similar temperature fluctuations can be potentially treated as a block of constant amplitude and constant frequency fatigue-like load. Finally, introducing few simplifying considerations, it has been assessed that the simulated behavior is coherent with the theoretical one coming from exploiting well-established thermo-based methods.

1. Introduction

Wood is a natural renewable material that has been used by humanity for numerous daily functions since ancestral times. Its capacity to be cut into different shapes and abundance at many latitudes have contributed to its constant search and use. The fact that wood is prone to change its form under specific environmental conditions (*i.e.*, moisture, temperature and loading) has also enabled the development of many artefacts of refined geometrical configuration. These characteristics are identified through many applications such as domestic furniture or objects of cultural heritage, sport products, building structures and interiors. However, despite its strengths and characteristics, wood is a climate-susceptible material which swells or shrinks by exchanging moisture with the surrounding environment, due to temperature (T) and relative humidity (RH) fluctuations [1,2] which can be caused by the natural microclimate variability or by artificial perturbations induced using Heating, Ventilation and Air Conditioning (HVAC) systems. Studies in literature have been focused on investigating the climate-dependent behavior of wood, wooden objects and structures to assess the material degradation, crack formation and damage mechanisms due to environmental changes. Dietsch et al. [3] carried out one-year measurements of the climatic conditions and of the moisture content of several different timber structures; they found out that the prevalent type of damage was the formation of cracks parallel to the wood grain, caused by severe changes of moisture content. In [4] Schellen and van Schijndel proposed a way to minimize the thermo-hygro-mechanical stress in wooden interior parts, using a building model for simulating the indoor microclimate and the moisture transport related to T and RH fluctuations in lime wood cylinders. In [5–7], analytical and experimental evaluations have been carried out on

* Corresponding author.
E-mail address: chiara.bertolin@ntnu.no (C. Bertolin).

https://doi.org/10.1016/j.finmec.2023.100186
Received 11 February 2023; Received in revised form 7 March 2023; Accepted 8 March 2023
Available online 20 March 2023

slices of *Scots pine* wood with the aim of quantifying the climate stress induced by a single hygric variation monitored over time. In particular, the studies have been based on monitoring the hygro-mechanical reactions of wood by means of acoustic emissions, which highlighted the stress released in form of acoustic waves at the formation of macro-cracks.

However, the timescale of diffusive phenomena in a wooden material induced by microclimatic variations is usually long (the order of magnitude is of dozens of days, if not months) and, so, experimental and monitoring campaigns of case studies are rare and time consuming. Among the longest monitoring campaigns, some remarkable results have been proposed in literature. For example, Bratasz et al. [8] monitored for more than two years the dimensional response of a wooden altarpiece in the Church of Santa Maria Maddalena in Rocca Pietore (Italy), where the indoor microclimate is perturbed by artificial heating episodes, causing abrupt variations of T and RH. It has been observed that the altarpiece experienced not only dimensional changes but also the opening and closing of a 2–3 cm deep crack in wood. Lucero-Gomez et al. [9], by means of a two-years monitoring campaign inside the Scuola Grande San Rocco in Venice (Italy) were able to extract the indoor environmental and to propose a climatic excursion index for investigating the entity, time and number of fluctuations affecting a selected microclimate. In a recent work [10] Califano et al. analyzed the microclimatic data coming from an almost three-years monitoring campaign carried out in Ringebu stave church (Norway). This typical kind of building is almost completely made of wood and hosts numerous wooden works of art and heritage objects belonging to Medieval times. For this reason, based on evidence available in literature, a simple method for evaluating the hygro-mechanical stress developed in wooden elements subjected to microclimatic fluctuations has been proposed. However, as stated before, due to the timescale and duration of moisture-related phenomena, monitoring campaigns are generally limited to few-years-long time-windows. Therefore, the long-run effect of repeated and persistent microclimatic loads has been hardly investigated up to now. In addition, to the knowledge of the authors, no studies are available on the long-run effect of 30 years of use of sporadic heating strategies in heritage buildings, as churches for example. In this framework, the current work proposes a preliminary data-driven methodology for approaching the issue of climate-induced fatigue on wood and wooden materials. The selected study case and location is Ringebu stave church (Norway), which has been object of previous investigations and results [5,10,11]. The timeseries of outdoor T and RH in Ringebu location have been downloaded from open-source platforms for different time periods and have been used, together with monitored data belonging to the Symbol and Spara Och Bevara projects,[1] to establish a computational approach able to reconstruct the timeseries of T experienced inside the considered building, namely Ringebu stave church (Section 2.1). The reconstructed indoor temperature timeseries have been analyzed and a simple logic for extracting the T increments from the timeseries has been proposed (Section 2.2). At this point, after introducing some simplifying assumptions, a preliminary approach for the assessment of the climatic fatigue of wood has been proposed, inspired by existing well-established methods [12,13] (Section 2.3). The implementation of the above methods has led to promising outcomes in terms of timeseries reconstruction (Section 3.1), natural climate-induced fatigue (Section 3.2) and the effect of artificial-climate perturbations superimposed to the natural ones (Section 3.3), over the horizon of 30 years in the far past (*i.e.*, 1948–1977), in the recent past (*i.e.*, 1981–2020) and in the far future (*i.e.*, 2071–2100). Finally, some general considerations about the above approach applied to the field of conservation are provided (Section 3.4), together with concluding remarks and future perspectives (Section 4).

[1] https://www.ntnu.edu/symbol; https://sparaochbevara.se/

2. Materials and methods

This Section deals with the description of the methodologies implemented for:

- **reconstructing the indoor temperature time series**, based on the outdoor one. The outdoor temperature data in Ringebu (Norway) location have been downloaded from the NASA's *Giovanni*[2] web-based application, which provides many Earth science remote sensing data, for the period of time that goes from 1948 to 2010, with a time resolution of three hours). Outdoor temperature data in Ringebu location for the far future (from 2071 to 2100, with a time resolution of one day) have been downloaded as well. In particular, concerning the future timeseries, the projections of climate change forced with different greenhouse gas (GHG) emission scenarios and impacting on Ringebu stave churche outdoors have been assessed, using regional climate models (RCMs). These types of models were developed with the aim of downscaling climate fields produced by coarse resolution global climate models (GCMs) thereby providing information at fine, sub-Global grid scales, more suitable for studies of regional phenomena. Among these RCMs, in this study, the COSMO COnsortium for Small-scale Modelling (CCLM) developed in 2008 by Rockel et al. [14] for climate predictions in the far future. CCLM is a non-hydrostatic model able to produce weather forecasts. The selected Representative Concentration Pathway (RCP) scenario was the RCP4.5 - stabilization scenario [15]. The CCLM model, receiving as input the downscaled GCMs data (*e.g.*, precipitation, air temperature and potential evapotranspiration (calculated)), and parameters which describe the catchment areas, allowed the forecasting of hydrologic parameters over the FF periods.[3] In addition, both indoor and outdoor temperature data collected in Ringebu stave church (located in Norway) during the monitoring campaign belonging to the Symbol and Spara Och Bevara projects[1] (March 2019 – March 2022) have been used for tuning the reconstruction tool;
- **analyzing the reconstructed indoor timeseries** for gathering information about the number and entity of the fluctuations affecting the indoor microclimate;
- **analyzing the problem of climate-induced fatigue** with a simplified approach.

2.1. Indoor time series reconstruction

The reconstruction of an unknown internal time series is done in two phases. The first phase, also called *tuning phase*, finds the time constants of the transfer function simulating the buffer behavior of the considered building between outdoor and indoor environments; specifically, both an internal and the corresponding external time series are needed for this step. The tuning of the transfer function is done by iteratively trying different time constants and check which parameters give a better reconstruction. In other words, the known external time series is given as input to the transfer function, together with time constants, to provide a synthetic internal time series as output. At this point, the synthetic series is compared to the known measured internal one. The tuning phase is carried out by using as input and output data the temperature timeseries collected during the monitoring campaign in Ringebu church, from March 2019 to March 2022. In the second phase, called *reconstruction phase*, the tuned transfer function is used to reconstruct internal

[2] https://giovanni.gsfc.nasa.gov/giovanni/

[3] The CCLM datasets for RCP4.5 with 1 km x 1 km grid spatial resolution analyzed for the Ringebu church location (Innlandet region, Norway) is available at the website of the Norwegian Water Resources and Energy Directorate, https://www.nve.no/.

time series from outside ones, which have been not used for the tuning phase. In this case, the input data are the past and future outdoor timeseries downloaded from the above-mentioned web platforms.

It is known from the literature [16,17] that an external time series applied to the right transfer function can become a good representation of the internal unknown one. Obviously, neither the shape of the transfer function nor the values of poles and zeros are known. For this reason, two complementary approaches for the transfer function estimation will be presented: a model-based approach and a computational one.

2.1.1. Model-Based approach

The model-based approach gives a solid physical interpretation of the desired behavior and gives a robust justification about the shape of the transfer function chosen for the purposes of the work. According to this approach, any building can be modelled as a box: the four walls of the box and the roof are in contact with the external environment that acts as a thermal bath. The thermal bath is represented by the air outside the church at temperature T_{out}. Consequently, there is heat exchange between the building and the environment through the walls. In addition, the floor is in contact with the soil; however, even though the soil itself can be treated as a thermal bath, the common sense teaches that the temperature of the floor inside a room is similar to the indoor temperature rather than to the outdoor one. However, it is clear that there is heat exchange between the floor and the soil, and that there is heat exchange between the soil and the air of the surrounding environment as well. As these processes are much slower than the others, they can be neglected. For the sake of simplicity, in this work, solar radiation and other heat sources have been neglected as well.

The simplest linear model that can be used for characterizing the above phenomenon is constituted by a system of two ordinary differential equations (ODE), defined as follows:

$$\begin{cases} \dot{x} = (f - x)/\tau_f + (y - x)/\tau_y \\ \dot{y} = (x - y)/\tau_y \end{cases} \tag{1}$$

where x $\equiv T_{in}$, being T_{in} the temperature inside the church; f $\equiv T_{out}$, being T_{out} the temperature outside the church; y $\equiv T_{floor}$, being T_{floor} the temperature of the church floor;

τ_y = time-scale of the floor-church heat exchange;

τ_f = time-scale of the environment-church heat exchange.

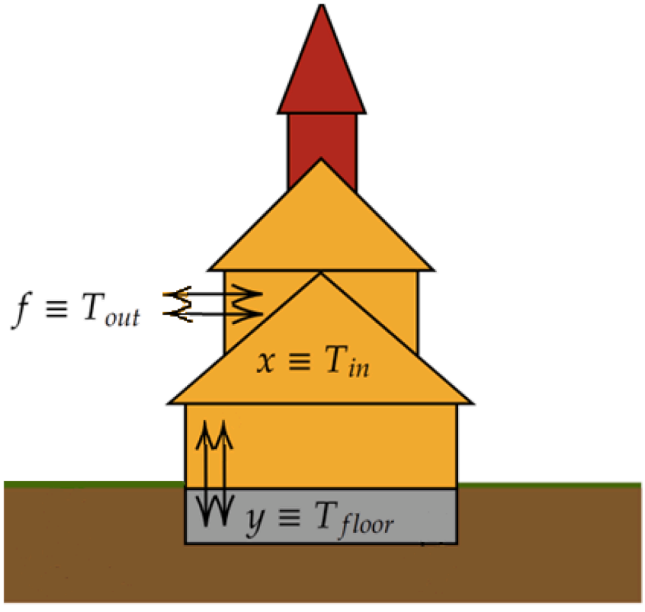

Fig. 1. Schematization of a generic building (in this case, Ringebu church - Norway) with the main heat exchange processes in act.

A simple schematization of a building (Ringebu stave church, in this case), with the acting heat exchange processes, is represented in Fig. 1 with the same symbols as described above.

Applying the Laplace transform $\{x(t) \overset{\mathscr{L}}{\rightarrow} \widehat{X}(s); f(t) \overset{\mathscr{L}}{\rightarrow} \widehat{F}(s)\}$, it can be easily obtained

$$\widehat{X}(s) = \frac{s\tau_y + 1}{s^2\tau_y\tau_f + (2\tau_f + \tau_y)s + 1}\left[\widehat{F}(s) + \widehat{CI}(s)\right] \tag{2}$$

where the initial conditions, $\widehat{CI}(s)$, can be expressed as

$$\widehat{CI}(s) = x_0\tau_f + \frac{\tau_f y_0}{s\tau_y + 1}, \tag{3}$$

and where x_0 and y_0 are the initial values for $x(t)$ and $y(t)$ respectively.

The obtained transfer function $G(s)$ has one zero, τ_y, and the following two poles

$$\tau_\pm = \frac{2\tau_y\tau_f}{2\tau_f + \tau_y \pm \sqrt{4\tau_f^2 + \tau_y^2}}. \tag{4}$$

In particular, if $\tau_f \gg \tau_y$, Eq. (4) becomes

$$\tau_\pm \approx \frac{2\tau_y\tau_f}{2\tau_f + \tau_y \pm 2\tau_f\left(1 + \frac{\tau_y^2}{8\tau_f^2}\right)} = \begin{cases} \tau_+ \approx \tau_y/2 \\ \tau_- \approx 2\tau_f \end{cases} \tag{5}$$

while, in the opposite scenario, if $\tau_y \gg \tau_f$

$$\tau_\pm \approx \frac{2\tau_y\tau_f}{2\tau_f + \tau_y \pm \tau_y\left(1 + \frac{2\tau_f^2}{\tau_y^2}\right)} \approx \begin{cases} \tau_+ \approx \tau_f \\ \tau_- \approx \tau_y \end{cases}. \tag{6}$$

Finally, the $G(s)$ can be written as

$$G(s) = \frac{s\tau_y + 1}{(s\tau_+ + 1)(s\tau_- + 1)} \approx \frac{s\tau_y + 1}{s\tau_- + 1} \tag{7}$$

since, in both cases, $\tau_- \gg \tau_+$. However, only the first case, Eq. (5), is physically feasible since the second case, Eq. (6), would lead to $G(s) = 1$.

Therefore, this physical model predicts that the transfer function will have one zero and two poles; if one dynamic process is slower than the other, the transfer function can be approximated with Eq. (7). It has to be noted that this physical model is useful for determining the shape of the $G(s)$ but it does not allow to compute the time constants.

2.1.2. Computational approach

The fundamental idea behind this second approach is defining the formulation of the optimal $G(s)$ by trying different functional forms of the $G(s)$ itself and, for each attempt, performing a complete grid-search over the parameters space, with the final aim of finding the minimum of a specified loss function. In particular, the loss function is the L_2 loss between the indoor temperature time series, T_{in}, and the reconstructed one, T_{in}^{rec}. is

$$L_2 = \sum_{i=1}^{N} \|T_{in} - T_{in}^{rec}\|^2 \tag{8}$$

where N is the number of samples in the available time series, T_{in}.

At this point, testing different transfer functions of small complexities up to the following form with four time constants

$$G(s) = k_{stat}\frac{(s\tau_1 + 1)(s\tau_3 + 1)}{(s\tau_2 + 1)(s\tau_4 + 1)} \tag{9}$$

a grid-search has been performed, and the results obtained for the different forms of transfer function are reported in Table 1.

From Table 1 it can be appreciated that the optimal model is the one with one zero and two poles

Table 1
Optimal parameters for G(s). The error near the value of the parameter is the grid width of the grid search.

$G(s)$	τ_1	τ_2	τ_3	τ_4	k_{stat}	*L2-loss*
k_{stat}	0	0	0	0	1.02 ± 0.01	437,610
$k_{stat}\frac{1}{(s\tau_2+1)}$	0	15.4 ± 0.01	0	0	1.07 ± 0.01	83,828
$k_{stat}\frac{1}{(s\tau_2+1)(s\tau_4+1)}$	0	15.3 ± 0.1	0	0.034 ± 0.001	1.07 ± 0.01	84,367
$k_{stat}\frac{(s\tau_1+1)}{(s\tau_2+1)}$	5.02 ± 0.01	22.5 ± 0.1	0	0	1.08 ± 0.01	57,517
$k_{stat}\frac{(s\tau_1+1)}{(s\tau_2+1)(s\tau_4+1)}$	6.19 ± 0.01	0.62 ± 0.1	0	24.2 ± 0.1	1.08 ± 0.01	57,102
$k_{stat}\frac{(s\tau_1+1)(s\tau_3+1)}{(s\tau_2+1)(s\tau_4+1)}$	9.9 ± 0.1	25.2 ± 0.1	2.4 ± 0.1	4.9 ± 0.1	1.05 ± 0.01	61,728

$$k_{stat}\frac{(s\tau_1+1)}{(s\tau_2+1)(s\tau_4+1)} \tag{10}$$

and it is compatible with the physics-based model found in Section 2.1.1. In case the two timescales are substantially different from each other, *i.e.* $\tau_f \gg \tau_y$, the $G(s)$ with the best performance is the one with one pole and one zero

$$k_{stat}\frac{(s\tau_1+1)}{(s\tau_2+1)} \tag{11}$$

which, from Table 1, is the second best according to the L_2-loss value.

It is worth to mention that the physics-based model has three time-constants, but only two are independent, indeed τ_y and τ_f. Instead, the model in Eq. (10) has three independent time-constants, thus showing a higher complexity. Therefore, the physics-based model is useful for determining the shape of the transfer function but then, the poles and zeros are considered independent. According to the physics-based approach, a suitable model is well-represented by a transfer function that has no more than one zero. Therefore, a more complex function would not provide additional benefits, as underlined in Table 1.

It has to be underlined that the grid-search has been performed by hand, just looking at the direction of the parameters that minimizes the loss function. This approach has been lately justified by inspecting the loss function landscape and noticing that it is a smooth surface, as clearly visible in Fig. 2; therefore, this assures that there are no sub-optimal minima. This can be done as, implicitly, the L_2-loss is a function of the parameters of $G(s)$, *i.e.,* $L_2(\tau_1, \tau_2, \tau_3, \tau_4, k_{stat})$.

2.1.3. *Indoor temperature timeseries reconstruction*

Since the purpose of the work is to reconstruct the indoor temperature timeseries starting from the outdoor one, in principle, once the $G(s)$, resembling the buffer behavior of the building between the outdoor and indoor environments, is known, the first step of the work is completed. However, there could be the possibility that the parameters of the $G(s)$ are over-fitted, *i.e.* they are tailored on the actual considered timeseries without generalizing well the properties of the building under concern (Ringebu stave church, in this case).

In other words, it could happen that, for different timeseries (collected in different periods of the year and/or in different years) related to the same case study, the tuned parameters of the $G(s)$ are different. With the simplified hypotheses that no restoration/renovation interventions have been made to the building structure and that, during the years, the walls mechanical and thermal properties remain the same, the parameters of the $G(s)$ can be considered constant, with a good approximation. However, in the current case, as the tuning of the transfer function has been carried out over a relatively short period of time (namely, two months in summer), while the reconstruction needs to be carried out over a period of time of roughly a hundred years, a verification is mandatory. For this reason, Table 2 reports the results of the $G(s)$ tuning for different periods.

In general, monitoring data collected from March 2019 to March 2022 in Ringebu Church are affected by the artificial heating used in the Church itself. For this reason, only data related to limited time periods during which the artificial heating was not used (*i.e.,* in summer, in sporadic weeks/months of the year, during the COVID-19 lockdown in 2020) were considered for fitting the transfer function (Table 2). In this way, through the transfer function, it is possible to reconstruct the

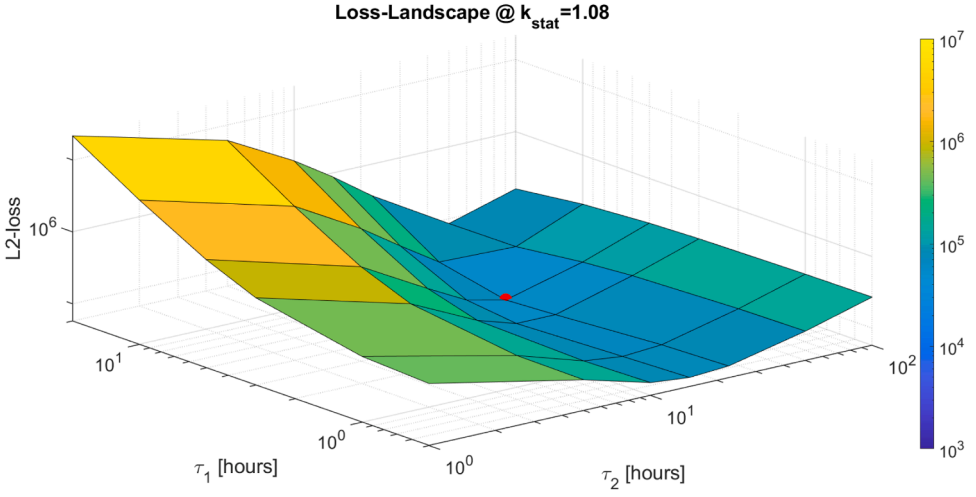

Fig. 2. Loss landscape of the G(s) with one zero (τ_1) and one pole (τ_2) for the Ringebu stave church. This loss is calculated on the time series June-August 2019. The red point is the optimum value (*i.e.*, minimum) for the loss function.

Table 2
Optimal parameters for different tuning periods. The error near the value of the parameter is the grid width of the grid search.

Date	τ_1	τ_2	k_{stat}	L2-loss	# points
2019/06 – 2019/08	5.02 ± 0.01	22.5 ± 0.1	1.08 ± 0.01	57,517	26,494
2020/06 – 2020/08	4.36 ± 0.01	21.7 ± 0.1	1.04 ± 0.01	54,440	26,494
2021/06 – 2021/08	4.04 ± 0.01	19.2 ± 0.1	1.03 ± 0.01	51,356	26,494
07–13/02/2020	2.5 ± 0.1	23.3 ± 0.1	0.82 ± 0.01	1530	1729
07–13/02/2021	2.4 ± 0.1	6.0 ± 0.1	1.00 ± 0.01	5370	1729
07–13/02/2022	4.4 ± 0.1	20.0 ± 0.1	0.79 ± 0.01	490.2	1729
15/03/2020 – 31/05/2020	2.7 ± 0.1	16.9 ± 0.1	1.00 ± 0.01	80,127	22,450

indoor natural microclimate, *i.e.,* the one that is not affected by artificial systems of heating/ventilation/conditioning.

From the results in Table 2, except for the period 07–13/02/2021, which is characterized by a quite small τ_2, all the parameters are coherent to each other for all the other periods. Even though the values themselves do not seem compatible in a strict sense, the Bode plot can help noticing that the various transfer functions are in agreement with each other (see Fig. A1 in Appendix). As the periods from June to August for the three years of the monitoring campaign (2019, 2020 and 2021) are those in which, for sure, the indoor Ringebu microclimate is completely natural because no heating, Ventilation and Air Conditioning (HVAC) systems are used, the average parameters computed over these three time periods, and reported in Eq. (12), are taken as benchmark for the subsequent evaluations

$$\begin{cases} \tau_1 = 4.47 \\ \tau_2 = 21.1 \\ k_{stat} = 1.05\ . \end{cases} \tag{12}$$

Going into the details of the implementation, the code has been written in MATLAB© and consists in: 1) a grid search of the parameters; 2) a Simulink simulation, for every proposed parameter. In this framework, two block-diagrams are used: one for tuning and one for reconstructing. The first one is shown in Fig. 3.

The Simulink circuit (Fig. 3) is made up of two main parts. In the upper part, the output time series is loaded and passed in input to the transfer function. A quantize block has been introduced in order to have a T_{in}^{rec} of the same type of T_{in}, *i.e.* as measured by the temperature sensor, having a resolution of 0.1 °C. In the lower part, instead, the L2-loss is calculated, and the results stored into the MATLAB© workspace. The second block-diagram is quite simple and is not shown herein. It only consists in the previously tuned $G(s)$, to which the current outdoor temperature timeseries (T_{out}) is applied, in order to reconstruct the indoor one. A fixed-step solver has been chosen with a time step based on the sampling time of the data: for the tuning part, the data has a sampling time of five minutes, equal to the data acquisition sampling used during the monitoring campaign; for the reconstruction part, the time series for the 1948–2010 period has a sampling time of three hours, equal to the sampling available in the data download platform (*Giovanni*). The results of the tuning phase are shown in Section 3.1.

2.2. Statistical indicators for time series characterization

Once the indoor temperature time series have been reconstructed, it could be useful to extrapolate the fluctuations experienced by T over the considered time periods. In particular, for this study, the interesting fluctuations are the T increments, as they bring to the dehumidification of the indoor environment which, without moisture content compensation, may cause deformations and damages (even failure) in moisture-sensitive materials (*e.g.,* wood).

To detect the temperature fluctuations, a simple and fast logic, proposed for the first time in [10] and herein modified, can be followed. Fig. 4 shows a chunk of indoor T timeseries represented by a blue curve along which two subsequent time-windows (blue and orange rectangles) of length L can be considered. The two time-windows share the *i* point of the timeseries; in particular, the first time-window (blue rectangle) covers the range of data going from $T_{i\text{-}L}$ to T_i, while the second time-window (orange rectangle) covers the range of data going from T_i to T_{i+L}. At this point, the two following quantities are introduced:

$$d1_i = avg\left(T_{[i-L,i]}\right) + std\left(T_{[i-L,i]}\right)$$

$$d2_i = avg\left(T_{[i,\ i+L]}\right) - std\left(T_{[i,\ i+L]}\right)$$

$$i = 1 + L,\ \ldots,\ N_{data} - L \tag{13}$$

where $avg\,(\ldots)$ and $std(\ldots)$ are the mean and the standard deviation of the considered timeseries chunk, and N_{data} is the number of data in the timeseries.

The quantity $d1$ is the sum between the average level of T and its

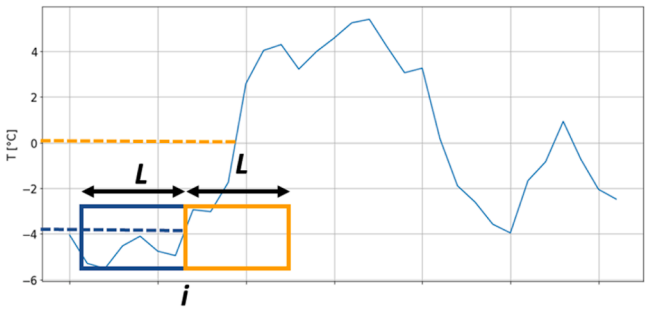

Fig. 4. Generic chunk of the indoor temperature timeseries (blue curve) with two subsequent time-windows (blue and orange) of length L that share the point i.

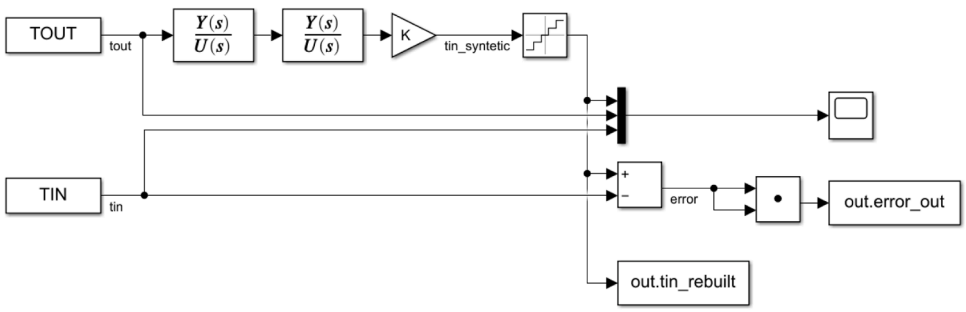

Fig. 3. Tuning Simulink circuit.

standard deviation, computed for the first time-window (blue dashed line in Fig. 4), while the quantity $d2$ is the difference between the average level of T and its standard deviation, computed for the second time-window (orange dashed line in Fig. 4). As a fluctuation of T is characterized by an abrupt variation of the general trend of T, the following quantity

$$V_i = |\min(d1_i - d2_i, 0)|. \tag{14}$$

can be introduced as useful tracer for the occurrence of T increments.

As a matter of fact, when T is increasing the quantity $d1_i - d2_i$ is negative and, therefore, the V_i is non null. In this way, a database of V_i is helpful in identifying all the increments of temperature highlighted by non-null values. The results in terms of V_i computed on a time-window with one day resolution are reported in Fig. 5, for an excerpt of timeseries going from 1948 to 2010.

By means of this simple statistical indicator, capable of quickly inspect long timeseries, it is possible to detect and collect all the increments of T experienced in the periods of interest, namely 1948–2010 and 2071–100. It has to be noted that this approach is carried out on the indoor temperature timeseries reconstructed through the methodology described in Section 2.1. This means that the indoor timeseries are representative of the natural microclimate that is theoretically experienced inside Ringebu church by the works of art and structural elements stored within the building. Indeed, as the indoor temperature has been reconstructed starting from the outdoor one, it does not account for the fluctuations and modifications introduced by the use of artificial heating which, in this particular church, is quite severe in cold periods of the year.

2.3. A simplified approach for the climate-induced fatigue

Exploiting the approach described in Section 2.2, it is possible to extract the entity of temperature increments from a timeseries. These temperature fluctuations, characterizing the indoor natural microclimate of the considered building, act as thermo-mechanical loads causing the arising of stress fields in climate-susceptible materials and components stored within the building. In [10] a simple analytical approach has been proposed for evaluating the stress levels arising in wooden samples due to microclimatic fluctuations. Therefore, based on analyses carried out in previous works [10,11], the considered case study is a circular slice of *Scots pine* wood (diameter = 16 cm, thickness = 2 cm) [5] which resembles a portion of a wooden sculpture, and which is assumed to be stored inside Ringebu church, thus being subjected to its indoor microclimate. Once the T fluctuations have been extrapolated from the timeseries, by means of the tool in [5,10], they can be translated into stress levels affecting the wooden slice. Therefore, as the natural microclimate shows different-frequency repetitive patterns (daily, seasonal and yearly fluctuations) [18], the linked stress levels are repetitive as well. In addition, as each microclimatic fluctuation works like a single loading-unloading cycle, the entire timeseries can be seen as a fatigue loading history. However, due to the different timescales of climatic phenomena, the actual fatigue loading history is characterized by both variable amplitude and variable frequency. For this reason, as the problem of climatic fatigue of wood is tricky and still poorly studied, in this work a preliminary and simplified approach is proposed.

For the current application, a useful methodology is the one proposed by Risitano et al. [12] for the evaluation of cumulative damage in materials (mostly metals and additively manufactured materials) subjected to fatigue. The method is based on the basic assumption that every component, if dynamically loaded, shows a surface temperature increment. This means that it is possible to associate a loading stress level with a temperature value. Despite the above method has been established and widely proven for metals and metallic materials over the years, its underlying idea is valid for the problem under concern, which deals with the analysis of stress levels linked to the increments of temperature caused by the natural microclimate variations experienced by materials stored within the considered church including wood, wooden objects and fixed components.

The Risitano method is based on the following experimental observation:

$$\Delta T_i \cdot N_{fi} = \Phi = constant \tag{15}$$

where ΔT_i is the surface temperature observed at the $i\,th$ stress level, N_{fi} is the number of cycles to failure at the $i\,th$ stress level, and Φ is the energy parameter for the selected material. According to Eq. (15), the energy parameter Φ is constant for a given material (once the fatigue loading has been fixed in terms of both loading ratio, R, and frequency, f) and is, therefore, represented by a rectangular hyperbola. Each point of such hyperbola is obtained by cycling a given material specimen with a constant amplitude loading until failure.

For applying this method to the problem under concern, it has to be noted that the sequence of temperature increments extracted by the microclimatic timeseries, resembling the loading history experienced by wooden materials and objects, is highly variable. Thus, the following considerations are made:

1) the temperature increments extracted through the method in Section 2.2 need to be rounded to the nearest integer, for the sake of simplicity. Each class of temperature increment occurs in the timeseries for a total number of times indicated as N;
2) similar rounded temperature increments that have a mutual time distance comparable to the minimum time resolution of the available time series can be considered as successive. Therefore, a sequence of successive similar temperature increments can be considered as a constant amplitude loading block;
3) in this preliminary approach, similar successive temperature increments are assumed to have the same duration, for the sake of simplicity. Therefore, a sequence of successive similar temperature increments can be considered as a constant amplitude and constant frequency loading block;
4) the number of successive similar temperature increments can be considered as the number of cycles (N_c) for the given loading block;
5) in absence of experimental and numerical evidence, the stress level associated to each temperature increment can be evaluated by using the analytical model proposed in [10].

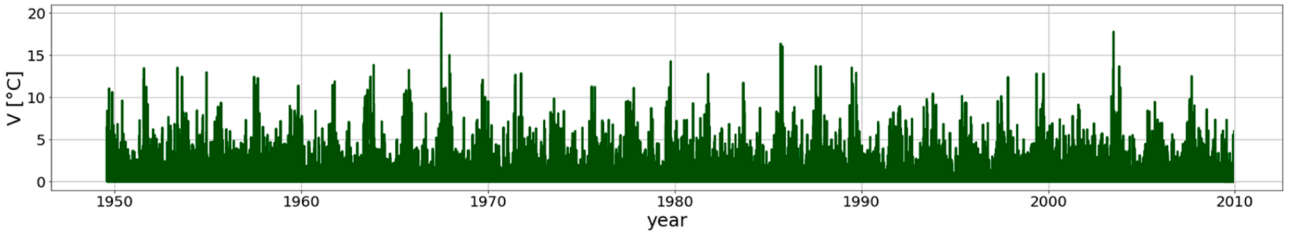

Fig. 5. V computed according to Eqs. (13)-14 with one-day long time-windows for the period of time going from 1948 to 2010.

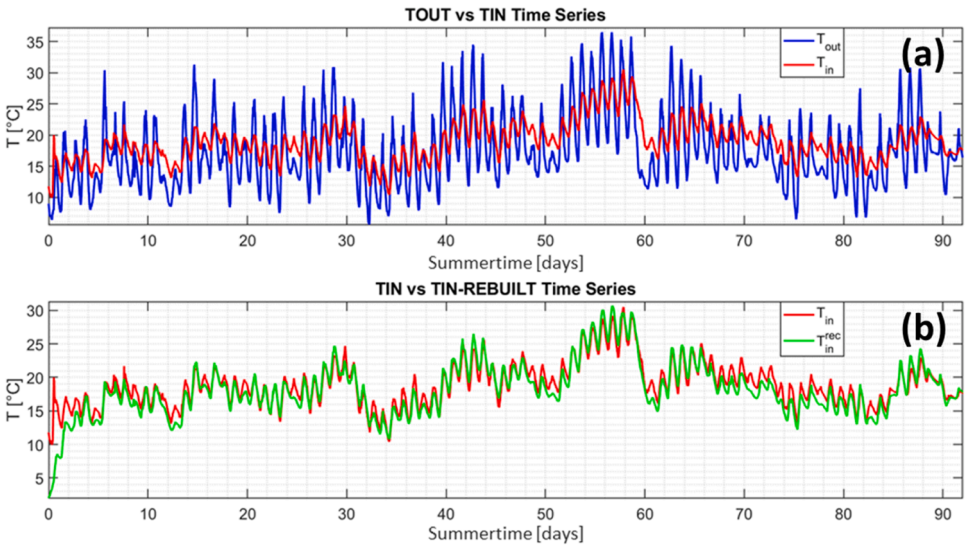

Fig. 6. Tuning results for the time series June-August 2019. (a) the outdoor monitored temperature (blue curve) and the indoor monitored temperature (red curve); (b) the indoor monitored temperature (red curve) and the reconstructed indoor temperature (green curve).

3. Results and discussion

3.1. Timeseries reconstruction

As described in Section 2.1.3, the outdoor-indoor transfer function has been tuned using data coming from the monitoring campaign carried out in Ringebu church from 2019 to 2022. *Fig. 6* shows the results of the tuning for the period June-August 2019. In particular, *Fig. 6*a shows the outdoor temperature (blue curve) and the indoor temperature (red curve) collected by the dataloggers installed during the monitoring campaign, while *Fig. 6*b shows the monitored indoor temperature (red curve, the same as the red curve in *Fig. 6*a) and the one reconstructed by means of the transfer function (green curve) for the same time period.

Once the transfer function has been tuned on the actual data collected during the monitoring campaign, it has been used to reconstruct the indoor temperature timeseries for the period 1948–2020 and for the far future scenario 2071–2100, providing as input data the outdoor temperature timeseries downloaded from online platforms, as described in Section 2. The results of the reconstruction are shown in Fig. 7 and Fig. 8 for the 1948–2020 and the 2071–2100 periods, respectively. Fig. 7a shows the outdoor temperature timeseries (blue curve) and the reconstructed indoor one (red curve) for the past (1948–2020), while Fig. 7b and Fig. 7c show two close-ups, in order to better visualize the timeseries: one for the decade 1970–1980 and one for the year 2003. Fig. 8 shows the outdoor (blue curve) and reconstructed indoor (red curve) temperature timeseries for the future.

3.2. Natural microclimate-induced fatigue

The main results obtained following the simplified approach

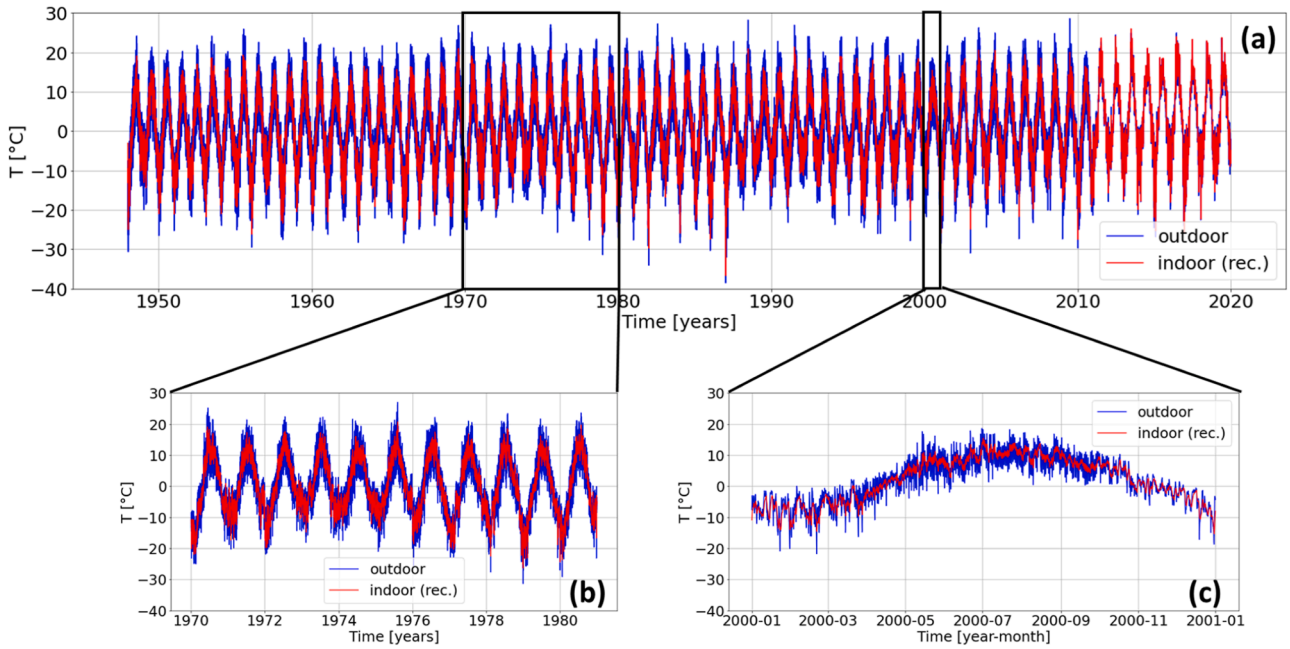

Fig. 7. Outdoor temperature timeseries (blue curve) and indoor reconstructed temperature timeseries (red curve) for the period going from 1948 to 2020 (a). Two close-ups are represented as well: for the period 1970–1980 (b) and the year 2003 (c).

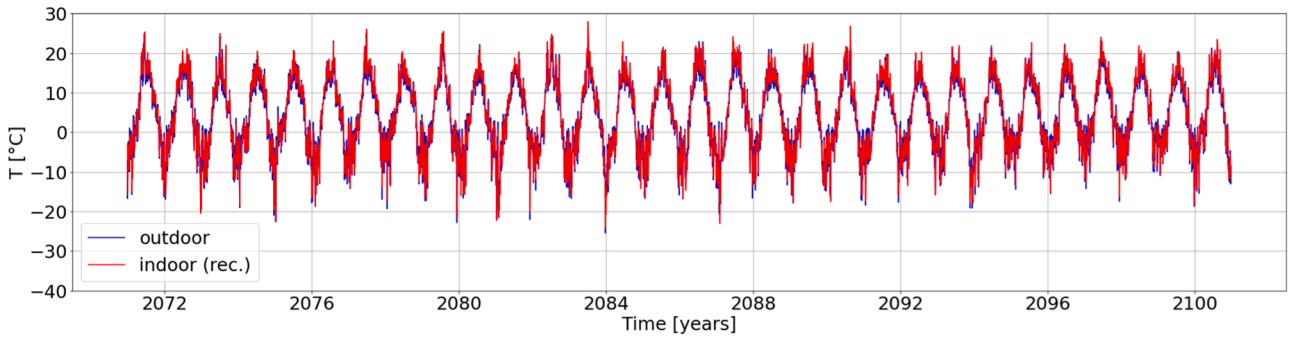

Fig. 8. Outdoor temperature timeseries (blue curve) and indoor reconstructed temperature timeseries (red curve) for the period going from 2071 to 2100.

described in Section 2.3 are reported in the following. It has to be noted that the results are shown for three different 30-year periods: 1948–1977, 1981–2010 and 2071–2100. This choice is related to the fact that in climatology and atmospheric sciences the microclimatic timeseries are, when possible, studied in periods of thirty-years.

According to consideration 1), the T increments extracted from the reconstructed timeseries, following the logic expressed in Eq. (13)-14, have been rounded to the nearest integer to easily find repeatability, and the number of occurrences (N) of each class of T increment has been computed. The rounded T increments (also named *Delta T* or DT) are reported in Fig. 9 through a bar plot representing their occurrences for the three different reference periods. In detail, the blue bars represent the increments for the far past (FP, 1948–1977), the green bars represent the increments for the recent past (RP, 1981–2010) and the orange bars represent the increments for the far future (FF, 2071–2100). It has to be underlined that the T increments for the three periods have been extracted considering timeseries with the same time resolution (one day), for the sake of consistency.

In the FP the bars distribution has the DT peak at 2 °C, while in the RP the bars distribution has major changes, respect to the FP, in the 1 °C $\langle$ DT $<$ 2 °C and DT $\rangle$ 8 °C ranges. Concerning the FF, the general trend of the bars distribution is characterized by lower N than those of the FP and the RP. The reason behind that is twofold: first, the time resolution of the FF timeseries is daily, hence some fluctuations could be hidden; second, the external forcing of climate change is expected to evolve to an increasing global warming, according to the projections of the RCP4.5. Indeed, the increasing evolution of the global temperature will lead to a generally indoor warmed and drier climate in which some fluctuations may be mitigated.

Preliminary evaluations on the climate-induced fatigue of wooden materials are shown in *Fig. 10* (in particular, *Fig. 10*b is just a close-up of *Fig. 10*a). The extracted loading blocks, as defined through considerations 2), 3) and 4), are represented with colored circles for the period 1948–1977 (blue), 1981–2010 (green) and 2071–2100 (orange). Each circle represents a block of Nc (with $Nc \leq N_{fi}$) successive cycles of similar *Delta T* obtained from the sequence of T increments extracted with Eq. (13) – 14. Due to a severe gap in literature about the fatigue of wooden materials subjected to climate-induced loadings, the present approach has been proposed as a quick and simple way for qualitatively assessing the constant amplitude and constant frequency fatigue. As the timescale of climate-induced phenomena is usually long (the order of magnitude of the diffusive behavior is of dozens of days, if not months), monitoring and experimental campaigns do not last as long as required for carrying out fatigue life assessments. Hence, as for the current case study the only evidence is obtained for single-event (*e.g.*, static) loadings [5,10] to be considered as the worst case scenario limit, the dashed curves in *Fig. 10* have been obtained by computing, according to Eq. (15), the energy parameter Φ for $Nc = N_{fi} = 1$ (representative of a static load, worst case scenario) at the most alarming ΔT_i (and associated stress) that caused failure. In case of uniquely natural microclimate, the most alarming ΔT_i is the highest one, as it is representative of the maximum fluctuation that is naturally experienced and that potentially needs to be, somewhat, mitigated. Then, the computed Φ has been used, together with each observed ΔT_i, to extrapolate each theoretical Nc ($= N_{fi}$). Each obtained curve is the theoretical locus of points of fracture for the selected time period. In addition, the continuous curves are the hyperbolic fits of the colored scatters which represent the Risitano-like curves, obtained with the hypotheses that the observed blocks of loading may

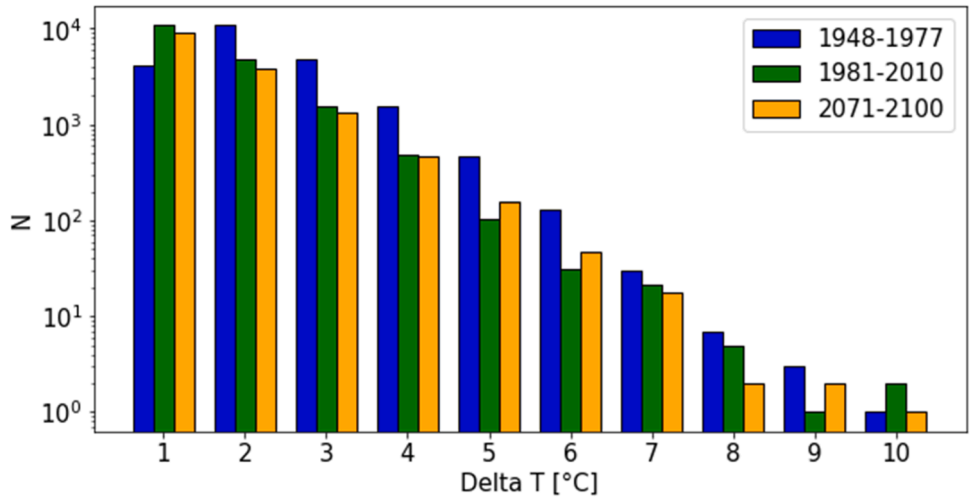

Fig. 9. Bar plot showing the occurrences (N) of the temperature increments (Delta T) caused by the natural microclimate for the three selected time periods: 1948–1977 (blue bars), 1981–2010 (green bars) and 2071–2100 (orange bars).

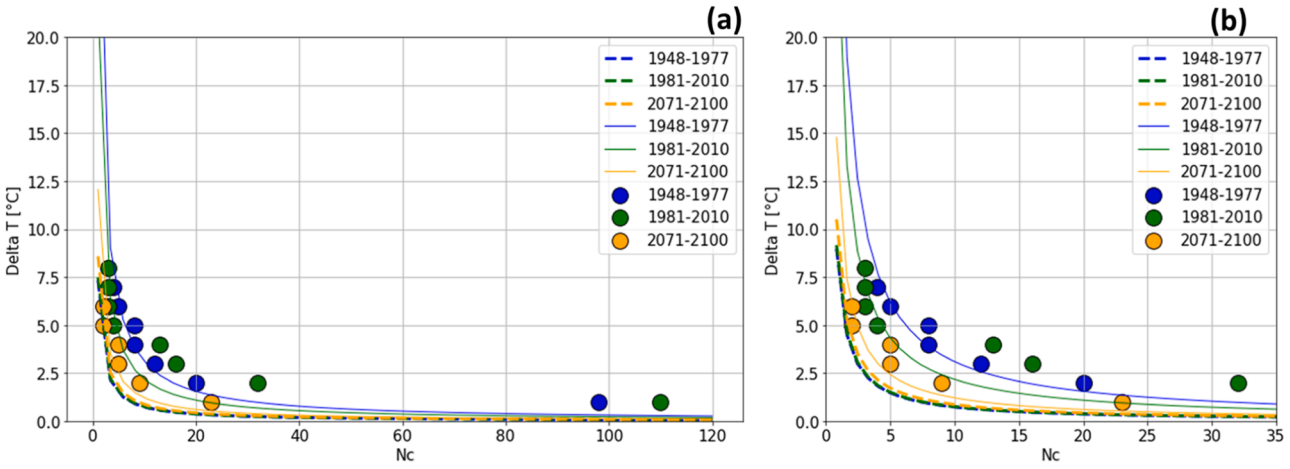

Fig. 10. Preliminary plots for the fatigue behavior of wood according to the thermo-based method [12], in case of completely natural microclimate. The colored circles represent loading blocks made by N_c similar successive *Delta T* for the three time periods. The continuous curves are the hyperbolic curves fitted on scattered data (circles) according to Eq. (15), while the dashed curves are the theoretical curves obtained according to Eq. (15) with the energy parameter computed for the static case. The subplot (b) is just a close-up of subplot (a) for better showing the behavior at low N_c.

cause failure.

As the energy parameter Φ, represented by the curves in *Fig. 10*, is the integral of the sample surface temperature over time up to fracture [12], the area under each continuous curve is proportional to the energy released during the selected fatigue test following the first micro-fracture. Hence, it can be appreciated that, ideally, if the wooden samples are fatigued with a loading made by the selected loading blocks (colored circles), the more time goes on (from FP to FF, passing through RP), the less energy is expected to be released at the first microfracture. This means that the FF fatigue behavior (continuous orange curve) is evolving towards the theoretical behavior (dashed orange curve) that somewhat represents the worst-case scenario, as it has been derived from the known conditions of static fracture.

It has to be underlined that *Nc* (Fig. 10) is different from *N* (Fig. 9) based on the different meaning that they have been given: the former provides information about the possibility of experiencing repeated similar Delta T, acting as a fatigue-like loading, while the latter provides a statistic of the total number of Delta T experienced over a period of time (far past, recent past, far future).

3.3. *Effect of artificial heating perturbations*

The evaluations carried out up to now referred to the indoor natural microclimate, reconstructed from the outdoor one and, therefore, without any artificial perturbation. However, the microclimatic timeseries collected during the 2019–2022 monitoring campaign, belonging to previous projects[2], are perturbed by the use of artificial heating inside Ringebu Church in the cold periods of the year [19]. This means that there is a superposition between the natural microclimate and the artificial increments of temperature caused by the sporadic use of artificial heating. These artificial T increments have been extracted from the monitored timeseries using the logic explained in Section 2.2 and it has been observed that, for each year of the monitoring campaign, the number and entity of *artificial* T increments is almost invariant. Hence, the T increments of a single monitored year have been considered as a typical sequence of increments (with an average value of 5.5 °C) caused by the use of artificial heating. As there is knowledge that the artificial heating was installed in Ringebu church in the 1980s, the sequence of artificial T increments has been superimposed to the sequence of natural T increments in the periods 1981–2010 and 2071–2100. At this point, the considerations in Section 2.3 have been applied to these new

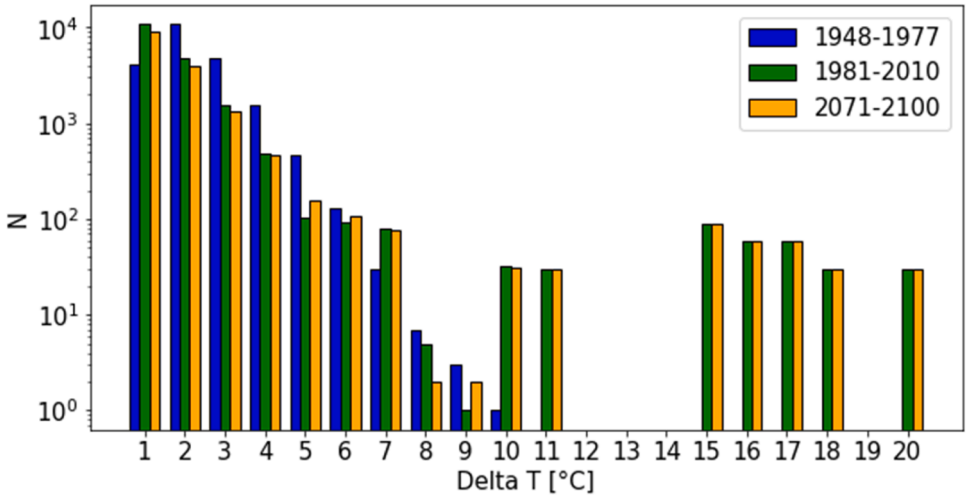

Fig. 11. Bar plot showing the occurrences (N) of the temperature increments (Delta T) caused by the microclimate for the three selected time periods: 1948–1977 (blue bars, only natural microclimate), 1981–2010 (green bars, mixture of natural and artificial microclimate) and 2071–2100 (orange bars, mixture of natural and artificial microclimate).

perturbed sequences and results as those shown in Section 3.2 have been obtained. As a matter of fact, Fig. 11, similarly to Fig. 9, shows the number of occurrences for each *Delta T*: the blue bars represent the increments for FP, the green bars represent the increments for RP and the orange bars represent the increments for FF. On the one hand, from Fig. 11 it can be easily noticed that, due to the perturbation caused by the artificial heating, the maximum experienced T increment is of about 20 °C; on the other hand, in Fig. 9 the maximum experienced T increment, in case of exclusively natural microclimate, is of about 10 °C, maximum. This highlights that the artificial perturbations of temperature, although being sporadic, are not negligible and induce a maximum thermo-mechanical load that doubles the one induced by the natural perturbations of temperature.

The superposition of Fig. 9 and Fig. 11 is shown in Fig. 12 for better visualizing the perturbations induced by the artificial heating (light green for the RP and light orange for the FF) respect to the ones induced by the natural microclimate (blue for the FP, dark green for the RP and dark orange for the FF).

It is clear that most of the *Delta T* induced by artificial heating are independent from those related to natural microclimate; only in the range 5 °C < DT < 10 °C it can be noted that, in some cases, the T increments generated by the use of artificial heating are comparable to those of the natural microclimate and, hence, it is possible to sum them up.

Similarly to *Fig. 10*, *Fig. 13* shows the loading blocks extracted from the T increments sequences, as defined through considerations 2), 3) and 4), for the period 1948–1977 (blue circles), 1981–2010 (green circles) and 2071–2100 (orange circles). The dashed curves are the theoretical Risitano curves obtained through Eq. (15) (worst case scenarios), while the continuous curves are the ones fitted on the scatters, following the same logic as that for *Fig. 10*. However, differently from what done for *Fig. 10*, in this case the most alarming ΔT_i is the lowest one, as it is representative of the minimum perturbation induced by the artificial microclimate which leads to static failure.

Focusing on the close-up in *Fig. 13*b, it can be seen that the theoretical curve for the FF (orange dashed curve, mixture of natural and artificial microclimate) falls completely below the theoretical curve for the RP (blue dashed curve, only natural microclimate). Taking into account the introduced simplifications and considerations, this means that in the FF, in presence of artificial heating perturbations, the occurrence of failure is expected to happen earlier (*i.e.*, at lower N_c and lower *Delta T*). This result seems to be realistic as artificial temperature perturbations can potentially be so severe to lead the wooden objects to premature failures.

It has to be noted that each circle in both *Fig. 10* and *Fig. 13* represents a block of *Nc* similar successive *Delta T*, resembling a constant amplitude fatigue loading block after which it is assumed to observe failure. However, as some of the most severe *Delta T* associated to the use of artificial heating are only sporadic, it is rare to find successive similar high *Delta T* in the typical yearly sequence. Due to this, in *Fig. 13* there are no markers in the area of temperature increments greater than 10 °C.

The considerations made up to know refer to the case in which each loading block (characterized by a given number, N_c, of *Delta T*) is considered independently from the others, as the current work proposes a preliminary way to address the problem of the climate-induced fatigue of wood.

However, a phenomenon that could significantly affect the fatigue life of wooden samples is the combination of a block of low *Delta T* followed by one single cycle at high *Delta T* (DT), namely the so-called "Low-High" fatigue. As a matter of fact, the presence of a single high impulsive load after a sequence of lower ones can be potentially disruptive [20,21]. In a real case study situation, as a heated church in this case, such Low-High fatigue episodes could happen in cold climates in wintertime (*e.g.* Scandinavian countries and mountain regions) when the indoor temperature is, on average, very low and excessive DT may be reached sporadically *e.g.*, during Christmas time), for the comfort of churchgoers, after a period of low DT (*e.g.* during typical Sunday services with low attendance and more sparing HVAC management done to reduce energy costs). However, this aspect is far beyond the object of this work and will surely be deepened in near future evaluations.

3.4. General considerations for the conservation of historic wood

The study of the climate-induced fatigue in wood is essential for providing insights about the conservation of wooden heritage objects and works of art (panel paintings, statues, furniture, ornaments *etc.*) disseminated all around the world. As a matter of fact, the works of art have been exposed to microclimatic fluctuations for decades or even centuries and this may lead to the arising of damage and micro-fractures. However, the problem of assessing and predicting the impact that repeated climate-induced loadings may have on such works of art is still scarcely explored. For this reason, the thermo-based preliminary approach herein proposed has the potential to estimate, in near future developments, the durability of wooden objects. Up to now, the investigated curves (*Fig. 10*, *Fig. 13*) make it possible to highlight the locus of conditions that, potentially, lead to surface micro-fractures linked to temperature increments. This means that the curve represents the set of microclimatic conditions that need to be avoided, or at least postponed

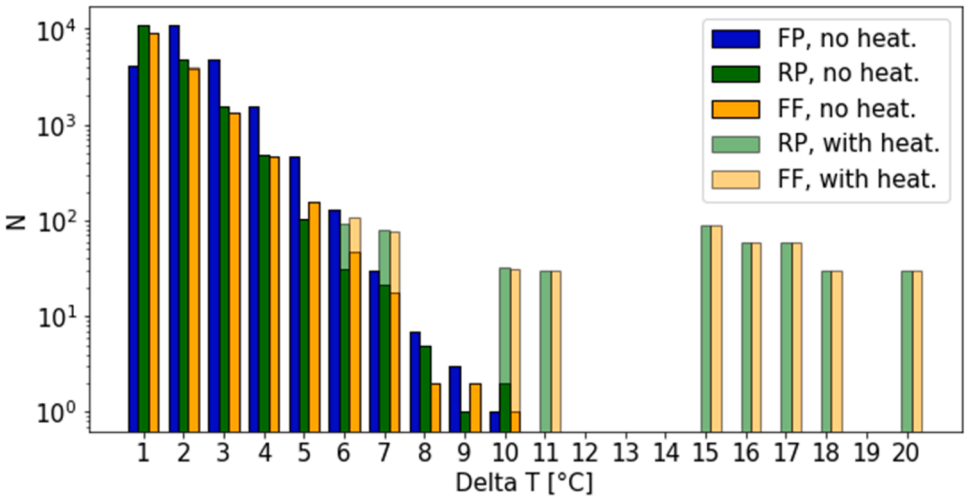

Fig. 12. Superposition of the bar plots of Fig. 9 and Fig. 11 in order to better visualize the effect of artificial heating. The dark colored bars represent the Delta T for the completely natural microclimate, while the light-colored bars represent the Delta T caused by the mixture of natural and artificial microclimate.

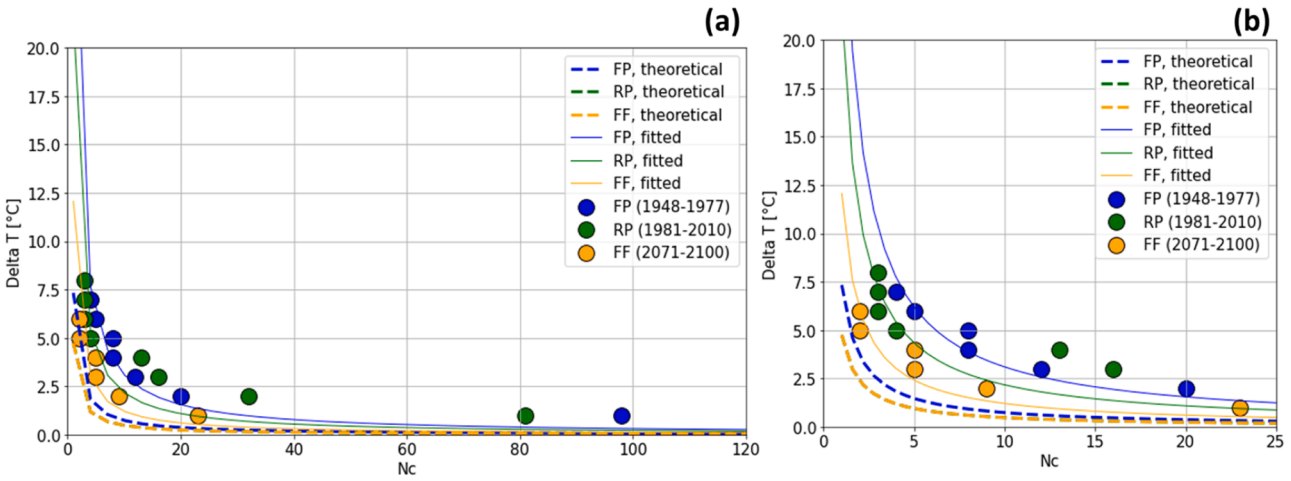

Fig. 13. Plots for the fatigue behavior of wood according to the thermo-based method [12] in case of both natural and artificial microclimate. The colored circles represent loading blocks made by N_c similar successive *Delta T* for the three time periods. The continuous curves are the hyperbolic curves fitted on scattered data (circles) according to Eq. (15), while the dashed curves are the theoretical curves obtained according to Eq. (15) with the energy parameter computed for the static case. The subplot (b) is just a close-up of subplot (a) for better showing the behavior at low N_c.

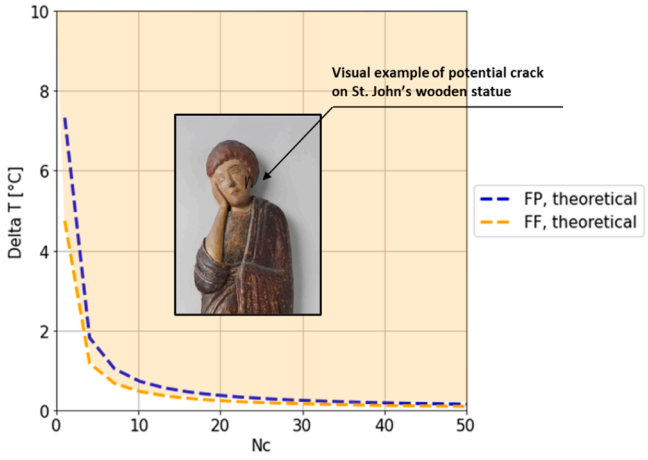

Fig. 14. Risitano-like curves and points of static failure for the FP, RP and FF with a representation of Saint John's statue (mid-13th century, Sculpture-Wood. Place: The Metropolitan Museum of Art, https://www.metmuseum.org/. https://library.artstor.org/asset/SS7731421_7731421_11764904) with the schematization of a potential surface crack.

as much as possible, by wisely using the HVAC systems, for example. As a matter of fact, if the conditions represented by the curves are met, surface fractures arise (Fig. 14 shows a visual example, for the sake of simplicity) and, above all, can propagate as time goes by.

The colored curves in Fig. 14 are the same dashed curves shown in Fig. 13: they are the theoretical Risitano curves obtained for the far past (1948–1977) and the far future (2071–2100). It can be noticed that, with the time passing by, the static failure condition is predicted to evolve to lower N_c and *Delta T*. This means that, if the predictions for the FF will effectively occur, the conditions represented by the orange curve are expected to be encountered earlier (namely, for lower temperature increments) if compared to FP. For this reason, to prevent the opening of microfractures on the wooden object's outer surfaces due to a mixture of natural and artificial temperature fluctuations, effective interventions on the use of HVAC systems need to be carried out in advance, on the basis of deeper evaluations about this topic that will be performed in the near future. However, it is clear that the investigations carried out up to now concerning the FF predictions need to be considered carefully as they are based on temperature timeseries obtained with a predictive model which, therefore, has intrinsic approximations. In near future evaluations, this approach could be potentially useful for discriminating among different conservation policies:

i) precautionary safety: there is not enough evidence about which risks are unacceptable and which bring to the climate-induced fatigue degradation on hygroscopic materials in case of wider temperature fluctuations allowed in museums, historic buildings, and archives to reduce the strict climate control and save energy;
ii) proven safety: the past climate load experienced by an object is fundamental for assessing whether future damage is likely to occur. Notwithstanding the impact of the ongoing climate change and the need of broadening climate control in museums and historic buildings, a more precise reconstruction of climate load experienced by valuable objects is needed.
iii) pragmatic risk management: the knowledge of the relationship among the hazard intensity, the damage, and the hazard control cost allows to limit the loss and to go in the direction of sustainable preventive conservation approaches. However, further research is needed to develop and validate damage functions capable to predict climate-induced fatigue on hygroscopic materials.

4. Conclusions

In this work, a preliminary approach for assessing the climate-induced fatigue of wood is proposed. As previous studies of the authors have been conducted on a slice of *Scots* pine, the same case study has been used in this investigation as well. In particular, it has been assumed that such sample is stored within the indoors of Ringebu stave church, an historic building located in Norway which hosts several wooden works of art (statues, furniture, ornaments etc.). In order to investigate the effect that repeated microclimatic loads potentially have on the wooden sample, the indoor microclimate of Ringebu church has been reconstructed. This has been carried out by fitting a proper transfer function, resembling the outdoor/indoor buffer behavior of the building, on outdoor and indoor temperature data collected during a monitoring campaign object of previous projects. The fitted transfer function has, then, been used for reconstructing the indoor temperature timeseries for three different time periods (far past, recent past and far future), providing as input data the outdoor temperature timeseries, for the analogous periods, downloaded from climatic data web platforms. The reconstructed timeseries have been analyzed and the recurring

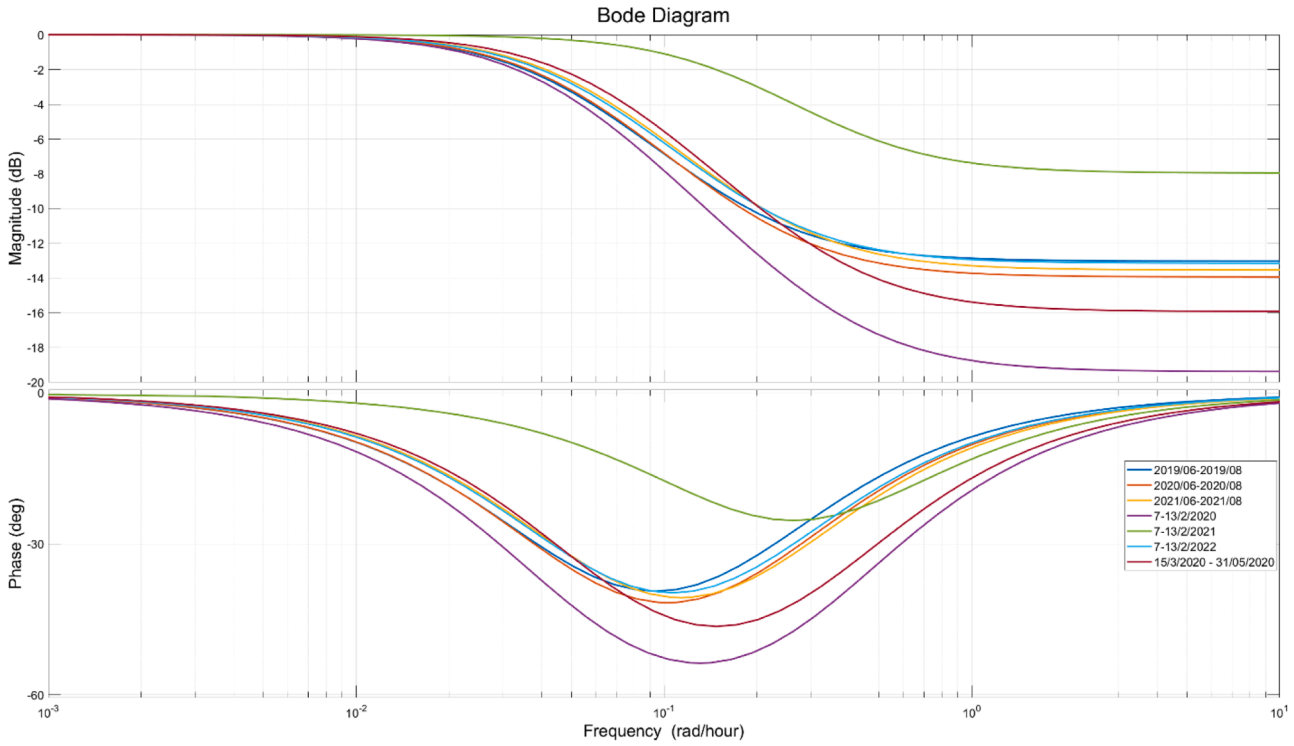

Fig. A1. Bode plot for the transfer function fitted on data belonging to different time periods, as defined in Table 2.

successive temperature fluctuations have been extrapolated, as they are the responsible for the wooden sample deformation. At this point, due to a severe gap in literature about the climatic-induced fatigue behavior of wood, a reliable and well-established method has been borrowed from fracture mechanics and it has been applied, with few simplifying considerations, to the case study under concern. According to this thermo-based fatigue method, preliminary considerations have been drawn on both the natural climatic fatigue of wood (*i.e.*, the one induced by the natural fluctuations of temperature) and the artificial one (*i.e.*, the one induced by repeated temperature fluctuations generated by the use of artificial heating systems inside buildings for improving the thermal comfort). It has been noted that, if successive similar temperature fluctuations are treated as a block of constant amplitude and constant frequency fatigue load, the obtained behavior is coherent with the theoretical one coming from the thermo-based method herein exploited, within the limits of the introduced approximations. However, at this stage, the loading blocks have been considered independent from each other. For this reason, near future perspectives will be based, first of all, on considering the effect of sequences of different loading blocks. In this way, the acquired knowledge will drive the research activities in the direction of variable amplitude climatic-fatigue. Then, introducing the duration and frequency of each loading cycle, it will be possible to approach and model the problem of variable frequency fatigue [22]. In this way, the outcomes and insights gained through these studies will potentially be useful for establishing effective practices and guidelines on how to avoid, or at least postpone, climatic conditions which may be harmful for the durability and structural integrity of wood and wooden valuable objects (panel paintings, statues etc.).

Declaration of Competing Interest

The authors declare the following financial interests/personal relationships which may be considered as potential competing interests:

Chiara Bertolin reports financial support was provided by Research Council of Norway. Chiara bertolin reports financial support was provided by Swedish Energy Agency.

Data availability

Data will be made available on request.

Acknowledgements

This work belongs to Sustainable Management of Heritage Building in a long-term perspective (Symbol) Research Project n. 274749 and to the Spara Och Bevara project n. 50049–1 and has been funded by the Swedish Energy Agency and the Norwegian Research Council.

Appendix

As described in Section 2, the transfer function simulating the building outdoor/indoor buffer behavior has been fitted on temperature timeseries collected during a monitoring campaign. Those data have been divided into different time periods and the transfer function has been fitted on all of them, in order to find the best fitting parameters.

References

[1] M.F. Mecklenburg, C.S. Tumosa, D. Erhardt, Structural response of painted wood surfaces to changes in ambient relative humidity, Paint. Wood Hist. Conserv. (1998) 464–483.
[2] E. Engelund Thybring, S. V Glass, S. L Zelinka, Kinetics of water vapor sorption in wood cell walls : state of the art and research needs, Forests 10 (2019).
[3] P. Dietsch, A. Gamper, M. Merk, S. Winter, Monitoring building climate and timber moisture gradient in large-span timber structures, J. Civ. Struct. Heal. Monit. 5 (2015) 153–165, https://doi.org/10.1007/s13349-014-0083-6.
[4] H.L. Schellen, A.W.M. van Schijndel, Setpoint control for air heating in a church to minimize moisture related mechanical stress in wooden interior parts, Build. Simul. 4 (2011) 79–86, https://doi.org/10.1007/s12273-011-0026-7.
[5] C. Bertolin, P. Karvan, F. Berto, Natural climate stress caused by a hygric change on coated pine samples: theoretical formulation and experimental validation, Eng. Fail. Anal. 129 (2021), https://doi.org/10.1016/j.engfailanal.2021.105669.
[6] P. Karvan, S.M.J. Razavi, F. Berto, C. Bertolin, Energy density and fracture parameters of coated scots pine, Constr. Build. Mater. 290 (2021), 123206, https://doi.org/10.1016/j.conbuildmat.2021.123206.

[7] C. Bertolin, L. de Ferri, F. Berto, Calibration method for monitoring hygro-mechanical reactions of pine and oak wood by acoustic emission nondestructive testing, Materials (Basel) 13 (2020), https://doi.org/10.3390/MA13173775.
[8] Ł. Bratasz, R. Kozłowski, D. Camuffo, E. Pagan, Impact of indoor heating on painted wood: monitoring the altarpiece in the church of santa maria maddalena in rocca pietore, Italy, Stud. Conserv. 52 (2007) 199–210, https://doi.org/10.1179/sic.2007.52.3.199.
[9] P. Lucero-Gómez, E. Balliana, F. Caterina Izzo, E. Zendri, A new methodology to characterize indoor variations of temperature and relative humidity in historical museum buildings for conservation purposes, Build. Environ. 185 (2020), https://doi.org/10.1016/j.buildenv.2020.107147.
[10] A. Califano, M. Baiesi, C. Bertolin, Novel risk assessment tools for the climate-induced mechanical decay of wooden structures: empirical and machine learning approaches, Forces Mech. (2022), 100094, https://doi.org/10.1016/j.finmec.2022.100094.
[11] A. Califano, M. Baiesi, C. Bertolin, Analysing the main standards for climate-induced mechanical risk in heritage wooden structures: the case of the Ringebu and Heddal stave churches (Norway), Atmosphere (Basel) 13 (2022), https://doi.org/10.3390/atmos13050791.
[12] A. Risitano, G. Risitano, Cumulative damage evaluation of steel using infrared thermography, Theor. Appl. Fract. Mech. 54 (2010) 82–90, https://doi.org/10.1016/j.tafmec.2010.10.002.
[13] A. Risitano, G. Risitano, Cumulative damage evaluation in multiple cycle fatigue tests taking into account energy parameters, Int. J. Fatigue 48 (2013) 214–222, https://doi.org/10.1016/j.ijfatigue.2012.10.020.
[14] B. Rockel, A. Will, A. Hense, The regional climate model COSMO-CLM (CCLM), Meteorol. Zeitschrift 17 (2008) 347–348, https://doi.org/10.1127/0941-2948/2008/0309.
[15] D. Jacob, J. Petersen, B. Eggert, A. Alias, O.B. Christensen, L.M. Bouwer, A. Braun, A. Colette, M. Déqué, G. Georgievski, et al., EURO-CORDEX: new high-resolution climate change projections for european impact research, Reg. Environ. Chang. 14 (2014) 563–578, https://doi.org/10.1007/s10113-013-0499-2.
[16] N. Manara, L. Rosset, F. Zambelli, A. Zanola, A. Califano, Natural climate reconstruction in the Norwegian stave churches through time series processing with variational autoencoders, Int. J. Build. Pathol. Adapt. (2022), https://doi.org/10.1108/IJBPA-01-2022-0017.
[17] *ASHRAE Handbook - HVAC Applications*, American Society of Heating Refrigerating and Air-Conditioning Engineers, 2011. ISBN 9781936504077.
[18] W. Anaf, O. Schalm, Climatic quality evaluation by peak analysis and segregation of low-, mid-, and high-frequency fluctuations, applied on a historic chapel, Build. Environ. 148 (2019) 286–293, https://doi.org/10.1016/j.buildenv.2018.11.018.
[19] P. Miglioranza, A. Scanu, G. Simionato, N. Sinigaglia, A. Califano, Machine learning and engineering feature approaches to detect events perturbing the indoor microclimate in ringebu and heddal stave churches (Norway), Int. J. Build. Pathol. Adapt. (2022), https://doi.org/10.1108/IJBPA-01-2022-0018.
[20] A. Califano, L. Grassia, A. D'Amore, Fatigue of composite materials subjected to variable loadings, J. Mater. Eng. Perform. 28 (2019) 6538–6543, https://doi.org/10.1007/s11665-019-04373-9.
[21] A. Califano, R. Dell'Aversano, Theoretical approach to the study of fatigue of composites under spectrum loading, AIP Conf. Proc. 1981 (2018), https://doi.org/10.1063/1.5046005.
[22] A. D'Amore, A. Califano, L. Grassia, Modelling the loading rate effects on the fatigue response of composite materials under constant and variable frequency loadings, Int. J. Fatigue 150 (2021), 106338, https://doi.org/10.1016/j.ijfatigue.2021.106338.